ELSEVIER

Polymer 42 (2001) 5823–5827

polymer

www.elsevier.nl/locate/polymer

Soft matter under osmotic stress

M. Leonard[a], H. Hong[b], N. Easwar[b], H.H. Strey[a,*]

[a]*Department of Polymer Science and Engineering, Box 34530, University of Massachusetts, Amherst, MA 01003, USA*
[b]*Department of Physics, Smith College, Northampton, MA 01060, USA*

Received 1 May 2000; received in revised form 1 December 2000; accepted 6 December 2000

Abstract

In this article, we will show that the osmotic stress method can be successfully applied to study the thermodynamics of self-assembly phenomena in soft matter systems, such as biopolymer liquid crystals, surfactant and lipid mesophases, and polyelectrolyte–surfactant complexes. We will give two examples to that effect. Firstly, we will present intercolumnar force measurements between cylindrical surfactant micelles in solid-state polyelectrolyte–surfactant complexes as a function of ionic strength. Secondly, we will present measurements of the DNA cholesteric spherulite structure and pitch as a function of osmotic pressure in an effort to evaluate the chiral contribution to the interaction between DNA molecules. © 2001 Published by Elsevier Science Ltd.

Keywords: Osmotic stress; Soft matter systems; Polyelectrolyte–surfactant complexes

1. Introduction

The theme of hierarchical self-assembly is ever-present in nature. Simple molecular building blocks such as amino acids, nucleic acids, lipids, and polysaccharides are assembled into ordered liquid crystalline arrays, intricately structured mesophases, and proteins. These entities are, in turn, self-assembled into larger-scale structures such as cell membranes, cartilage, bone, and cytoskeletal infrastructure.

The osmotic stress method provides a means for the direct investigation of the microscopic and thermodynamic details of these intermolecular interactions [1], and has been successfully employed to measure the intermolecular forces in lamellar stacks of lipid bilayers [2] and in hexagonal arrays of semi-stiff biopolymers, such as DNA [3], collagen [4], and various polysaccharides [5]. The essence of the method involves the controlled removal of water from samples in aqueous environments via the application of osmotic pressure from an inert species. The thermodynamic work required to remove the water from the sample is equivalent to the work required to push the molecules that constitute the structure closer together. In practice, the samples are equilibrated against a large excess of polymer solution whose osmotic pressure is known as a function of concentration, either through a dialysis membrane or across the solid–liquid phase boundary in phase-separated samples. Such an osmotic stress experiment is schematically illustrated in Fig. 1. Neutral and highly water-soluble polymers, such as poly(ethylene glycol) (PEG) and dextran, are well suited for use as osmotic stressing agents. For most charged biopolymer systems, higher-molecular-weight PEG is excluded from the interior of the sample as long as its radius of gyration is larger than the average distance between two polymer chains inside the sample [6]. Using polymer solutions, osmotic pressures from 1.0 kPa to about 30 MPa can be achieved and sample densities can be determined by X-ray scattering measurements of the intermolecular distances.

Using polymer solutions to apply osmotic stress has several advantages over the water vapor pressure method. While the osmotic pressure is set by the polymer concentration in the stressing solution, the salt activity can be fixed independently by adding salt to this solution. Because all activities are controlled by the stressing solution, the phase of the sample is precisely specified — there can be no phase coexistence. The absence of phase coexistence is crucial for determining the phase structure with X-ray scattering. The osmotic stress method also provides information about the free energy of the system, which can be obtained by integrating the equation of state [7].

2. Experimental

2.1. Materials

Poly(acrylic acid) (PAA), sodium salt (Aldrich, $\bar{M}_N = 2000$ g mol^{-1}, 40 wt.% solution in water), sodium bromide

* Corresponding author. Tel.: +1-413-577-1317; fax: +1-413-545-0082.
E-mail address: strey@mail.pse.umass.edu (H.H. Strey).

0032-3861/01/$ - see front matter © 2001 Published by Elsevier Science Ltd.
PII: S0032-3861(00)00903-4

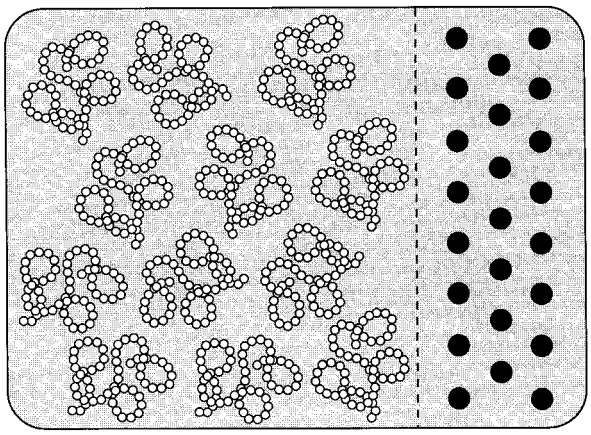

Fig. 1. Schematic illustration of an osmotic stress experiment. A large reservoir of stressing solution, consisting of PEG (white coils) dissolved in a salt solution (shaded background) is equilibrated through a semi-permeable membrane (dashed line) against an ordered sample (dark circles). If the sample and solution are phase-separated, the phase boundary replaces the semi-permeable membrane.

(Aldrich, ACS grade), sodium chloride (Mallinckrodt), sodium acetate (NaAc, Sigma), cetyltrimethylammonium chloride (CTAC) (Aldrich, 1.04 M solution in water), PEG (Fluka, $\bar{M}_N = 8000$ and 35,000 g mol^{-1}), and ethylenediaminetetraacetic acid (EDTA) (Sigma, molecular biology grade) were used as received. Tris(hydroxymethyl-aminomethane) (TRIS base) (Sigma, molecular biology grade) was adjusted to pH 7.0 (HCl) before use. Short fragment DNA was prepared from chicken erythrocytes using a previously described procedure [8].

2.2. Methods

Poly(acrylic acid)–cetyltrimethylammonium bromide (PAA–CTAB) complexes were prepared in polyethylene centrifuge tubes by adding 140 μl (7.56×10^{-4} mol charged units) of 40 wt.% polyelectrolyte solution to 1 μl (7.56×10^{-4} mol) of 1.04 M CTAC solution, followed by vigorous mixing. Upon the addition of approximately 10 ml water to this mixture, a fine white precipitate was formed. The precipitate was isolated by centrifugation, washed with three 50 ml aliquots of water, and allowed to air dry for approximately 8 h. Pieces of the dried complexes were then placed in aqueous sodium bromide solutions (10 and 100 mM) with PEG concentrations ranging from 0 to 50 wt.%. Each solution was buffered in a mixture of 10 mM TRIS base/1 mM EDTA. The samples were allowed to equilibrate with the stressing solutions for 2 weeks at room temperature. CTAB was generated in situ by the exchange of the CTAC chloride ion with the free bromide ions in the NaBr–PEG solutions.

DNA cholesteric droplets were prepared using the following procedure. Short fragment DNA was dissolved in 300 mM NaAc, 10 mM TRIS, and 1 mM EDTA at a DNA concentration of 5 mg ml^{-1}. DNA was precipitated and washed with a 75% ethanol/25% water mixture. Pellets (1 mg each) of short fragment DNA were dried in a Speed-vac (Savant Instruments). The pellets were re-suspended in 3–5 ml PEG solutions ($\bar{M}_N = 35,000$ g mol^{-1}), at concentrations ranging from 10 to 25 wt%, containing 0.5 M NaCl, 10 mM TRIS, and 1 mM EDTA. Cholesteric droplets were generated by gently shaking the samples after an equilibration time of 1 week.

2.3. Measurements

Small-angle X-ray scattering (SAXS) measurements were performed on a Rigaku RU-H3R rotating anode X-ray diffractometer equipped with an Osmic multilayer focusing optic and an evacuated Statton-type scattering camera. The sample-to-detector distance was 460 mm, which corresponds to a q range of $0.698\ \text{nm}^{-1} \le q \le 6.25\ \text{nm}^{-1}$ with $q = (4\pi/\lambda)\sin(\theta/2)$, where θ is twice the Bragg angle. The incident beam wavelength was 0.154 nm, corresponding to 8 keV Cu Kα radiation. Scattering patterns were acquired with 10×15 cm^2 Fuji ST-VA image plates in conjunction with a Fuji BAS-2500 image plate scanner, and intensity profiles were obtained from radial averages of the scattering pattern intensities.

Polarizing optical microscopy was performed with a Zeiss Axiovert S100TV inverted polarizing microscope (objective: Zeiss Plan-Neofluar $40\times/0.85$ pol) equipped with an LC Pol-Scope retardance imaging system (CRI, Boston, MA) which simultaneously measures the magnitude and direction of birefringence. Birefringence images $I(x, y)$ of individual cholesteric droplets were Fourier transformed $I(q_x, q_y)$ and the pitch was measured using the location of the first maximum in the angular averaged power spectrum $I(q)I^*(q)$ with $q^2 = q_x^2 + q_y^2$.

3. Results and discussion

3.1. PAA–CTAB complexes

An excellent example of electrostatic self-assembly is embodied in solid-state polyelectrolyte–surfactant complexes [9]. At appropriate polyelectrolyte concentrations [10] and charge densities [11], water-insoluble, long-range ordered structures form by combining both the components at a stoichiometric charge ratio. Periodicities in the nanometer range can be achieved with these materials [9] and the degree of order is generally quite high, as observed with SAXS.

Although charge neutralization plays a role in the thermodynamics of the polyelectrolyte–surfactant complex assembly, the principal driving force for this process is entropic in nature. Prior to complexation, the counterions are restricted to regions close to the surfaces of both the surfactant and the polyelectrolyte chain. Upon adsorption of a polyelectrolyte chain to the surface of the ionic surfactant, the bound counterions are released into solution from

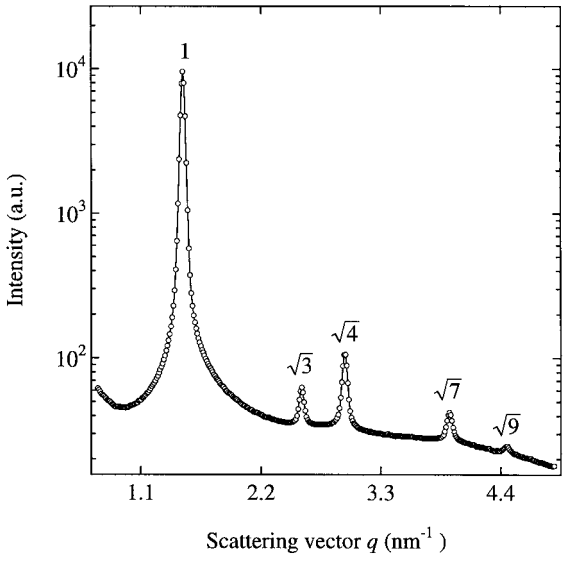

Fig. 2. Representative SAXS intensity profile for PAA–CTAB complex in 10 mM NaBr. The peak positions correspond to the *hk*0 diffraction signals of a hexagonally close-packed cylindrical structure.

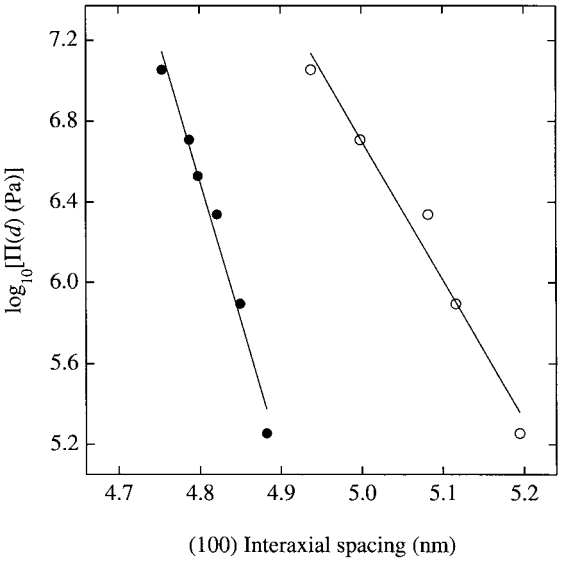

Fig. 3. Forces between CTAB cylinders in PAA–CTAB complexes bathed in 10 mM NaBr (filled circles) and 100 mM NaBr (open circles) at 25°C. The data shown here follow an exponential decay with decay lengths of 0.031 and 0.063 nm for the 10 and 100 mM NaBr solutions, respectively.

the surfactant surface and the chain, which, considering the extremely large number of freed counterions, gives rise to a significant increase in the overall entropy of the system. It is this increase in counterion entropy upon polyelectrolyte adsorption that drives the complexation process.

During complexation, the surfactant molecules assemble into spherical micelles, cylindrical micelles, or membranes, thus forming a crystalline lattice that defines the complex morphology. The polyelectrolyte binds to the surfaces and fills the space between the surfactant moieties. The structure of the material can be modified after complexation, however, and is dependent on such factors as ionic strength, salt type, and osmotic pressure.

Since the water-insoluble polyelectrolyte–surfactant complex phases are well-defined and since SAXS can be used as a structural probe for these systems, the osmotic stress method provides an attractive means to measure the repulsive intermolecular forces directly, and under thermodynamically well-defined conditions. To this end, a model system, consisting of PAA–CTAB complexes in sodium bromide solutions, was chosen and the complex structures were monitored as a function of ionic strength and osmotic pressure.

The complexes exhibited a hexagonally close-packed cylindrical phase over an osmotic pressure range of 0–12 MPa and at ionic strengths of 10 and 100 mM. Fig. 2 shows a representative SAXS profile for the complexes considered in this study. The peak positions represent the *hk*0 reflections one would expect for a long-range ordered, hexagonal array of cylinders. CTAB exists in a hexagonally close-packed cylindrical phase at its experimental concentration in sodium bromide solution [12] and it is these CTAB cylinders which are responsible for the hexagonal order of the complex. It is important to mention that the complexes self-assemble into highly ordered arrays immediately upon mixing since the same degree and type of hexagonal order was observed even in the absence of the stressing polymer.

Osmotic stress data for the PAA–CTAB complexes are given in Fig. 3. Each point represents the distance between the CTAB cylinders in a particular complex, as determined from the (100) X-ray diffraction signal measured at the corresponding osmotic pressure. Interaxial distances were calculated as $(2/\sqrt{3})d_{(100)}$. At each ionic strength, the interaxial forces are exponential, with decay lengths of 0.031 and 0.063 nm for 10 and 100 mM NaBr, respectively. Thus, a 10-fold increase in ionic strength causes the decay length to double. This translates into increased compressibility at higher ionic strengths: compression occurs over a 0.02 nm range in the 100 mM NaBr environment, where compression over a 0.01 nm range is observed at 10 mM NaBr. As the ionic strength is reduced, the interaxial spacings become smaller. This is reasonable, considering that at higher ionic strength the entropic driving force for the release of counterions upon adsorption of the polyelectrolyte chain will be reduced. Since fewer binding sites will be vacated by the departing counterions, the polyelectrolyte will naturally have fewer surfactant binding sites available to it upon adsorption. Therefore, more of the polyelectrolyte chain will be allowed to explore the interstitial space, which leads to an increased distance between the surfactant moieties at higher ionic strengths.

At this point, it is not clear to us what molecular length scale the measured exponential decay lengths correspond to. The decay lengths do change with ionic strength, but in an

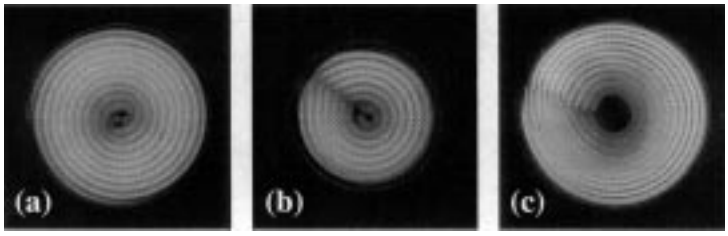

Fig. 4. Cholesteric DNA spherulites bathed in PEG ($\bar{M}_N = 35,000$ g mol^{-1}) solutions of increasing concentration at pH 7.5, 0.5 M NaCl, and: (a) 11% PEG; (b) 16% PEG; and (c) 17% PEG. The distances between the striations represent a cholesteric pitch of 2.4 μm for each of the spherulites shown.

opposite direction to that which one would expect for a Debye screening length. More experiments at different polymer molecular weights and charge densities have to be performed to determine precisely how the decay length depends on the environmental parameters of the system.

3.2. DNA cholesteric pitch measurements

Liquid crystals of DNA are the simplest model systems for DNA packing in nature, as observed in cell nuclei and bacteriophage heads [13]. In monovalent salt solutions, DNA exhibits the following sequence of liquid crystalline phases with decreasing DNA concentration [14]: crystalline (hexagonal, orthorhombic), hexagonal, line hexatic, cholesteric, blue phase, and isotropic.

Despite our knowledge about the structure of single DNA molecules, it is not completely clear how they interact inside the DNA liquid crystals. To illustrate this, consider the DNA cholesteric phase in 0.5 M NaCl, for which the average interaxial distance between molecules ranges from 3.5 to about 5.5 nm, and where the Debye screening length is 4.2 nm. This results in a typical surface to surface distance from 1.5 to 3.5 nm, assuming a DNA diameter of 2.0 nm. Thus, under these conditions, the average distance between the DNA surfaces is about 3–8 times larger than the screening length. If DNA molecules encounter one another through electrostatic interactions, why do DNA liquid crystals exhibit cholesteric twist?

The answer may be found in the equation of state for DNA liquid crystals. Recently, it was shown that there is a fluctuation-enhanced repulsion between DNA molecules, which dominates the interaction for interaxial distances greater than 3.5 nm [6,7]. The fluctuation-enhanced repulsion is entropic in origin and results from the bending fluctuations of DNA molecules which experience screened electrostatic repulsion. A similar mechanism could explain why there are chiral interactions between DNA molecules. Even though DNA molecules are far apart on an average, because of bending fluctuations, they occasionally come close enough to experience strong electrostatic repulsion, and consequently, chiral interactions. The question then presents itself: are there fluctuation-enhanced chiral interactions?

To address this question, we have systematically measured the DNA cholesteric pitch as a function of osmotic pressure and ionic strength. The solution properties of DNA, such as its helical pitch and charge density, are well known [15]. By studying the cholesteric pitch and liquid crystalline defect structures as a function of salt concentration and DNA density, we hope to connect the microscopic helical structure to the long-range order of its mesophase [16].

Representative defect structures of DNA cholesteric spherulites [17] at three different DNA densities are shown in Fig. 4. These spherulites form in the presence of the PEG stressing solution because of surface tension between the solution and the cholesteric DNA liquid crystal. At low DNA densities, a double spiral structure is found (Fig. 4(a)). The defect line in the middle is a diametrical χ disclination line of strength = 1, running perpendicular to the viewing plane and penetrating through the full diameter of the spherical DNA droplet.

At higher DNA densities, radial χ disclination lines of strength = 2 are found (Fig. 4(b) and (c)). When the cholesteric to hexatic (or hexagonal) transition is approached, the middle part of the cholesteric turns black, which suggests that the inside may be nematic, oriented perpendicular to the viewing field. The cholesteric liquid crystalline bending stiffness seems to be enhanced close to the transition as the central twist-layers bend with a smaller radius of curvature, expelling cholesteric twist from the regions whose radii are smaller than some critical value.

Fig. 5 shows the DNA cholesteric pitch of spherulites as a function of applied osmotic pressure. At low osmotic pressures, the cholesteric pitch seems to be independent of osmotic pressure whereas towards the cholesteric to hexagonal transition, the pitch diverges [18]. Above 19% PEG (pitch = 5.3 μm) the cholesteric phase ceases to exist, indicating a discontinuous jump to infinity in the cholesteric pitch as the hexagonal phase is approached.

From such pitch measurements combined with X-ray diffraction to determine the DNA interhelical distances [7], we will be able to measure the average twist angle between DNA molecules as a function of salt concentration and interhelical distance. Together with new theoretical insights into the nature of chiral interactions [19], we hope to be able to make the connection between microscopic and macroscopic mesophase chirality.

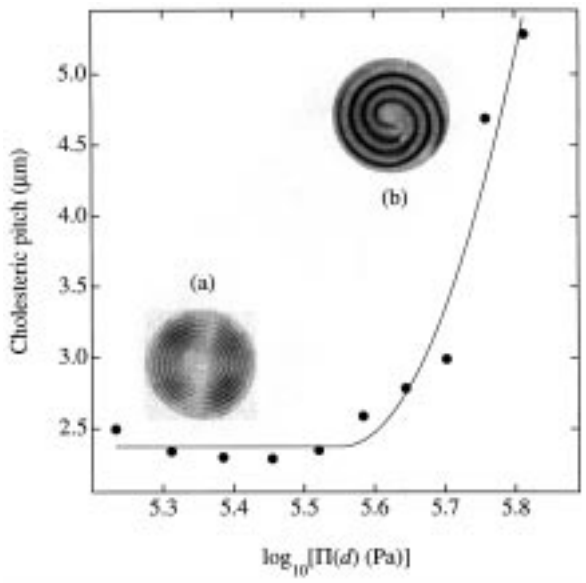

Fig. 5. Cholesteric pitch of DNA liquid crystals versus osmotic pressure in 0.5 M NaCl. Inset shows polarizing optical micrographs of the corresponding cholesteric DNA droplets: (a) 11% PEG; and (b) 19% PEG.

4. Conclusions

We have demonstrated the great potential of the osmotic stress method for the study of the thermodynamics and self-assembly of soft matter. Osmotic stress measurements can be used to measure directly the forces between macromolecules and supramolecular assemblies, and consequently their free energy of compaction as a function of parameters such as composition and salt activity. We can, therefore, test and compare the theories that predict the free energies of self-assembled systems, or provide high-quality data for systems where no such theories yet exist.

Acknowledgements

We gratefully acknowledge the National Science Foundation for supporting this work through the University of Massachusetts, Amherst, MRSEC and NSF Career award DMR-9984427.

References

[1] Parsegian VA, Rand RP, Fuller NL, Rau DC. In: Packer L, editor. Methods in enzymology. Orlando, FL: Academic Press, 1986. p. 400.
[2] Lis LJ, McAlister M, Fuller N, Rand RP, Parsegian VA. Biophys J 1982;37:657.
[3] Rau DC, Lee BK, Parsegian VA. Proc Natl Acad Sci USA 1984;81:2621.
[4] Leikin S, Rau DC, Parsegian VA. Nat Struct Biol 1995;2:205.
[5] Rau DC, Parsegian VA. Science 1990;249:1278.
[6] Strey HH, Parsegian VA, Podgornik R. Phys Rev Lett 1997;78:895.
[7] Strey HH, Parsegian VA, Podgornik R. Phys Rev E 1999;59:999.
[8] Shindo H, McGhee JD, Cohen JS. Biopolymers 1980;19:523.
[9] Ober CK, Wegner G. Adv Mater 1997;9:17.
[10] Ilekti P, Piculell L, Tournilhac F, Cabane B. J Phys Chem B 1998;102:344.
[11] Zhou SQ, Burger C, Yeh FJ, Chu B. Macromolecules 1998;31:8157.
[12] Auvray X, Petipas C, Anthore R, Rico I, Lattes A. J Phys Chem 1989;93:7458.
[13] Rill RL, Strzelecka TE, Davidson MW, Van Winkle DH. Physica A 1991;176:87.
[14] Livolant F, Leforestier A. Prog Polym Sci 1996;21:1115.
[15] Bloomfield VA, Crothers DM, Tinoco I. Nucleic acids: structures, properties, and functions. Sausalito, CA: University Science Books, 2000 (chap. 11).
[16] Sato T, Nakamura J, Teramoto A. Macromolecules 1998;31:1398.
[17] Bouligand Y, Livolant F. J Phys 1984;12:1899.
[18] Van Winkle DH, Davidson MW, Chen W, Rill RL. Macromolecules 1990;23:4140.
[19] Harris AB, Kamien RD, Lubensky TC. Phys Rev Lett 1997;78:1476.